Scene-to-Scene classification variability in spatiotemporal glacier surface facies mapping in Svalbard

Sagar Filipe Wankhede[1,3], Christo Jolly[1*], Keshava Balakrishna[1**], Shridhar Digambar Jawak[1,2]

[1]*Department of Civil Engineering, Manipal Institute of Technology, Manipal Academy of Higher Education, Manipal 576104, Karnataka, India*
[2]*Atmosphere and Climate Department, The Climate and Environmental Research Institute NILU, PO Box 100, NO-2027 Kjeller, Norway*
[3]*Government College of Commerce and Economics- Borda (Autonomous), Margao 403601, Goa, India*

Abstract

Spatiotemporal analysis of glaciological phenomena provides a robust assessment of a glacier's health. Glacier surface facies (GSF) are direct indicators of the state of snow and ice within a glacier. However, long-term analyses of GSF via optical satellite products presents challenges stemming from data availability, weather conditions, and variations in mapping methodologies. In this study we present the first decadal analysis of GSF in Svalbard using optical satellite data. Utilizing unsupervised classification on images of the Vestre Broggerbreen glacier from 2013 to 2023, we identify and quantify the variations between facies observed on the images and their classified spatial distributions. The identified facies comprise of snow, firn, glacier ice, and dirty ice, with a fifth thematic class of shadowed snow. In certain imagery, snow and firn are labelled as 'snow 1' and 'snow 2' due to the derived reflectance and appearance of firn differing from established patterns in the literature, while remaining spectrally distinct from snow. Our analysis suggests that shadowed snow induces the most misclassification in overall assessment of GSF. Shadowed snow and dirty ice produce convoluted spectral reflectance that in combination with the overall darkening of the glacier severely misrepresented firn, underreported dirty ice, and produced inaccurate maps. Spatially, dirty ice was classified with a lower distribution in 2023 (0.49 km^2) than in 2013 (0.58 km^2). Moreover, firn/snow 2 was classified as a larger area in 2023 (1.01 km^2). These results indicate a pressing need to identify long-term trends affected by scene-to-scene distortions. Our future experiments involve multi-decadal supervised analyses of GSF in the high Arctic involving image-specific discussions, thereby providing crucial information for refinement of supraglacial monitoring with multispectral data.

Key words: spatiotemporal analysis, ISODATA classification, glacier dynamics, image distortions, Svalbard, glacier facies

DOI: 10.5817/CPR2025-1-7

Received May 4, 2025, *accepted* August 30, 2025.
[*]Corresponding author: Jolly[*]<christocj75@gmail.com>; Balakrishna[**]<k.balakrishna@manipal.edu>
Acknowledgements: The authors thank HOD, Civil Engineering, and Director, MIT for their encouragement for this research. DEMs provided by the Polar Geospatial Center under NSF-OPP awards 1043681, 1559691, 1542736, 1810976, and 2129685.

Introduction

The cryosphere is the Earth's frozen component comprising ice and snow. It exercises a crucial function in the global climate. Glaciers are large persistent bodies of ice and snow formed on land. The mass accumulation and melting of a particular glacier are primarily determined by the season, meteorological factors such as temperature and precipitation, and the topography of the area. Glaciers are extremely sensitive to temperature and display immediate responses to climatic changes. Therefore, monitoring glaciers and their responses to climate dynamics provides an assessment of the impact of climate change (Jawak et al. 2022b). A glacier can be broadly categorized into two zones – accumulation and ablation. The accumulation zone refers to the region where mass is accrued, and the ablation zone predominantly loses mass (Jawak et al. 2022d). The equilibrium line altitude is the transition zone between the accumulation and ablation zones (Pope and Rees 2014a). A glacier's evolving state from formation to ablation can be documented through the occurrence and prevalence of glacier facies.

Traditional methods for mapping glacier facies rely on field surveys and topographic maps. These methods are tedious and inefficient. Additionally, it is quite difficult to traverse inaccessible mountainous areas. Remote sensing (RS) is an effective and efficient technology to monitor glacial dynamics. Each facies possess unique spectral and spatial properties which are useful for their characterization (Jawak et al. 2022b). These properties can be exploited for monitoring facies using multispectral images (Pope and Rees 2014a) and synthetic aperture radar (SAR) composites (Engeset et al. 2002).

Glacier (glaciological) facies were introduced by Benson (Benson 1959) and modified by Williams et al. (1991). Glaciological facies are formed over time and represent distinct phases of precipitated snow, compacted ice, melted forms of both, entrained debris, deposited dust, and surface debris. Usually covered by seasonal snow, these facies are visible on the supraglacial terrain in summer once the transient snow has melted. At the supraglacial level in direct contact with the local weather, facies present varying manifestations which are characterizable in optical data. These manifestations are called glacier surface facies (GSF) (Jawak et al. 2022a). The properties of each GSF are based on moisture, texture, appearance, brightness, and mixture of dust and debris.

The most observed glaciological facies are dry snow, wet snow, ice, and dirty ice. Dry snow, located at the highest elevations, is formed from multi-year accumulation of snowfall that has not melted. Wet snow is the region where snowmelt has permeated into the snowpack. The lower boundary of the accumulation zone is called the snowline. Meltwater may percolate and emerge beneath the snowline which eventually freezes into superimposed ice. Glacier ice begins as accumulated snow that is compacted due to compression and moves downhill along the slope of the bedrock (Pope et al. 2013). Ali et al. (2017) observed that the distinct properties of facies result in differential melt intensity. Multispectral data capitalizes on these distinctions to enable thematic characterization.

Multispectral RS enables identification of Earth's features through visible and infrared electromagnetic radiation. Open-source datasets like the Sentinel series and Landsat archives provide a robust time series of data which are available at various levels of spatial resolution (Jawak et al. 2022a). In addition to providing the spectral reflectance of glaciological phenomena, multispectral data can be used to calculate albedo (Greuell and Oerlemans 2005), isolate of crevasses (Luckman et al.

2012), and prepare digital elevation models (Pope et al. 2013). There has been a steady improvement in optical sensor resolution from 10 m to <0.4 m over the past 20 years (García-Rubio et al. 2015).

Pope and Rees (2014a) used multispectral images to classify glacier facies of the Midtre Lovénbreen glacier (Svalbard) with the help of full-spectrum surface reflectance. Similar multispectral data driven attempts at one-time snapshot mapping of facies in Svalbard have been performed using pixel-based supervised methods (Jawak et al. 2022a, Luis and Singh 2020), and object-based methods (Jawak et al. 2022b). Efforts have been made to identify the influence of specific wavelength ranges on the characterization of facies (Jawak et al. 2022c). These attempts have tried to identify the best mechanism for deriving accurate facies maps. However, there are only a handful of attempts at spatiotemporal mapping of facies in Svalbard. Among these, Jawak et al. (2023) analyzed spatiotemporal changes in GSF of the Midtre Lovénbreen glacier (Svalbard) from 2017 to 2022 using a mix of Sentinel-2A and Landsat 8 data. Garg et al. (2022) mapped facies for the glaciers in Ny-Ålesund from 2016-2020 using SAR composites. Although not directly comparable to multispectral attempts, it is one of the two significant attempts at spatiotemporal characterization of facies in Svalbard.

Braun et al. (2007) found that the spatial distribution and occurrence of facies can serve for calibrating and validating distributed mass balance models. Spatiotemporal mapping of facies can provide a distinct advantage for determining changes within the glacier body using characterization approaches. While there have been a handful of attempts to conduct change detection studies for specific GSF in the Himalayas (Yousuf et al. 2019, Ali et al. 2017, Haq et al. 2021, Jawak et al. 2019, Yousuf et al. 2024) similar attempts must be performed in Svalbard and other glaciated areas. Moreover, research into variations in GSF present inherent challenges such as cloud cover, illumination angles casting shadows, and consistency of data with maximum ablation. Yousuf et al. (2019) describe the importance of reliable reference data for consistent GSF mapping. Further challenges occur due to the large number of sensor-specific mapping methods with untested transferability (Wankhede et al. 2023), difficulty in generalization across time (Jawak et al. 2022a), and variation among analysts tasked with generating training data (Jawak et al. 2022c).

Considering these limitations, the present study attempts to map the evolution of GSF of the Vestre Brøggerbreen glacier in Ny-Ålesund, Svalbard from 2013 to 2023 using unsupervised classification with a combination of Landsat 7, 8, and Sentinel-2A/B data. The primary objective for using unsupervised classification is to provide an image focused understanding of classification and misclassification in a GSF specific context. These results will potentially lead to enhanced knowledge for an image analyst when attempting to derive training data across time.

Study Area

Svalbard is an Arctic archipelago, situated between 75° and 81°N (Fig. 1). It is one of the largest repositories of Arctic ice with a 60% glaciated area, representing approximately 10% of the total Arctic glacier area. It is very sensitive to climate shifts due to its position at the north of the warm and highly saline north Atlantic current (Kohler et al. 2007). Due to this, Svalbard has a warm and variable climate compared to other Arctic regions. Recent studies (Jawak et al. 2022b, Isaksen et al. 2016, Lapointe et al. 2024) suggest that Svalbard is warming 2-3 times quicker than the global average. The temperature in Svalbard has increased by ~4°C over the past century (Lapointe et al. 2024). This warming is mainly due to Arctic amplification (Wickström et al. 2020). Arctic amplification occurs due to factors like CO_2 concentration in the atmosphere, change in sea-ice extent, increase in H_2O content in the atmosphere (Wickström et al. 2020), and albedo feedback (Serreze and Barry 2011).

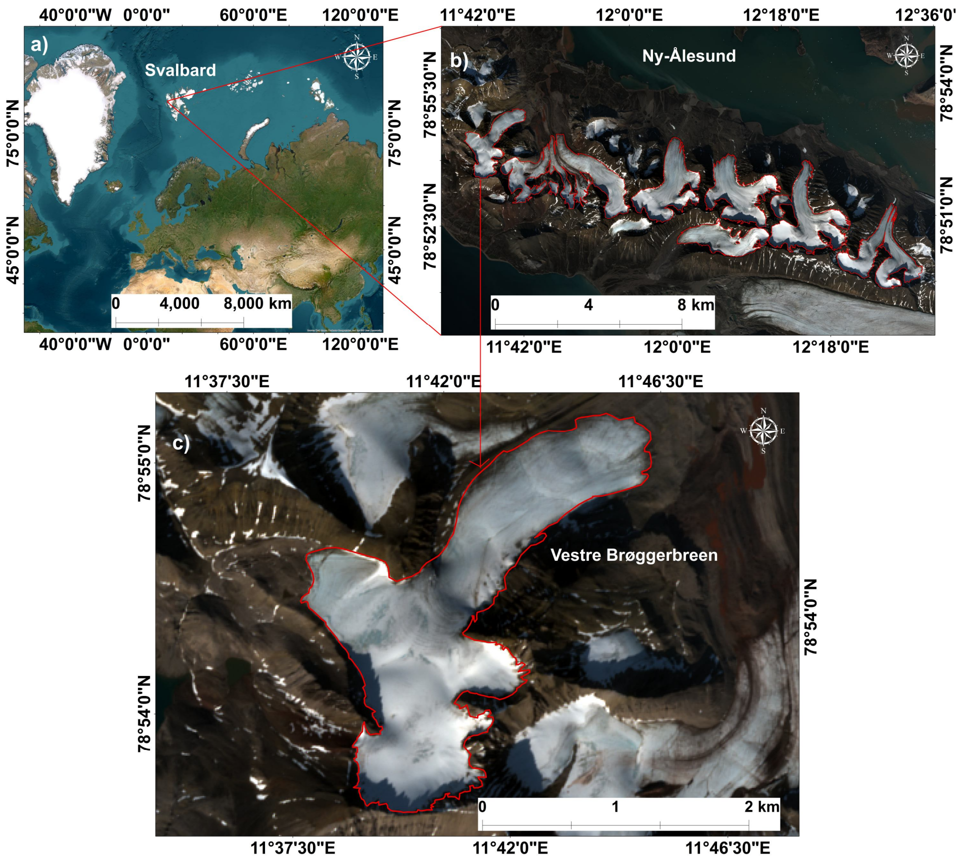

Fig. 1. Location of (a) Svalbard, (b) Ny-Ålesund, and (c) Vestre Brøggerbreen. The Svalbard inset is created using available basemap from ArcGIS. The insets of Ny-Ålesund and Vestre Brøggerbreen are prepared using Sentinel-2A data acquired in 2019.

This island group contains Ny-Ålesund, a research town with several international scientific stations. It is situated on the island of Spitsbergen, and it is the northernmost permanent settlement on the Earth (Kar et al. 2018). The glaciers in Ny-Ålesund are Austre Lovénbreen (AL), Vestre Brøggerbreen (VB), Austre Brøggerbreen (AB), Edithbreen (EB), Midtre Lovénbreen (ML), Pedersenbreen (PB), and Botnfjellbreen (BB). Vestre Brøggerbreen (VB) is a valley glacier located between 78°53′-78°56′ N and 11°36′-11°48′ E (Patel et al. 2019). VB is situated ~3.5 km southwest of Ny-Ålesund and divided into VB-I and VB-II with a medial moraine in between

(Sadiq et al. 2022). In the present study, we focus on VB-II, as it is the larger component. Geetha Priya et al. (2022) used an unmanned air vehicle to measure VB's surface melt for a four-day period. Other studies involve finding snow water equivalent (Patel et al. 2019), estimating glacier health using ice velocities (Sadiq et al. 2022), and biological studies (Kaštovská et al. 2005, Singh et al. 2016). While GSF have been mapped in Ny-Ålesund as a whole (Jawak et al. 2022a, 2022b), on ML (Pope and Rees 2014b) and EB (Luis and Singh 2020) in isolation, the present study is the first GSF characterization attempt focused on VB, and the first decade long spatiotemporal GSF analysis in Ny-Ålesund. Svalbard experiences summer from June-August with the warmest month being July and an average temperature of 5.6°C in Ny-Ålesund (Sadiq et al. 2022).

Datasets

The primary datasets for this study are Sentinel-2A/B images from Copernicus, Landsat 7 enhanced thematic mapper (ETM) + and Landsat 8 operational land imager (OLI) images from USGS. Table 1 presents the exact breakdown of the data across the temporal period of the study.

Sensor	Date of acquisition	Tile ID
Landsat 7 ETM+	14 July 2013	LE07_L2SP_220003_20130714_20200907_02_T1
Landsat 8 OLI	23 August 2014	LC08_L2SP_215004_20140823_20200911_02_T1
Landsat 8 OLI	01 August 2015	LC08_L2SP_216004_20150801_20200909_02_T1
Landsat 8 OLI	09 July 2016	LC08_L2SP_217004_20160709_20200906_02_T1
Sentinel 2B MSI	20 August 2018	S2B_MSIL2A_20180820T124659_N9999_R138_T33XVH_20230421T074221.SAFE
Sentinel 2B MSI	28 July 2019	S2B_MSIL2A_20190728T132729_N9999_R024_T31XFH_20230512T193109.SAFE
Sentinel 2A MSI	27 July 2020	S2A_MSIL2A_20200727T132721_N9999_R024_T31XFH_20230305T215438.SAFE
Sentinel 2B MSI	27 August 2021	S2B_MSIL2A_20210827T125709_N0500_R038_T33XVH_20230121T105836.SAFE
Sentinel 2B MSI	14 July 2022	S2B_MSIL2A_20220714T122659_N0400_R052_T31XFH_20220714T150159.SAFE
Sentinel 2A MSI	14 August 2023	S2A_MSIL2A_20230808T131721_N0509_R124_T31XFH_20230915T124603.SAFE

Table 1. Complete list of the sensor, date of acquisition, and tile IDs.

The scenes were selected after reviewing the maximum visible ablation, minimal cloud cover (less than 15%), low haze, and illumination angles. Based on these criteria, we could not find a suitable image for the year 2017.

All downloaded scenes were level 2 processed data (reflectance). Both Landsat sensors contain 7 multispectral wavelengths along with additional bands. However, Landsat 8 OLI has improved calibration, signal to noise cancellation and higher resolution when compared to Landsat 7 ETM+ (Roy et al. 2016). Sentinel 2 images comprise both Sentinel 2A and Sentinel-2B which have an identical sensor known as the multispectral instrument (MSI) and are phased at 180° to each other. Sentinel-2A/B consists of 11 multispectral bands with two additional spectrums. Table 2 presents the properties of each sensor, and the spectral bands used in the present study.

Sentinel 2A			**Landsat 8 OLI**			**Landsat 7 ETM+**		
Band	**Resolution**		**Band**	**Resolution**		**Band**	**Resolution**	
	Spectral (µm)	**Spatial (m)**		**Spectral (µm)**	**Spatial (m)**		**Spectral (µm)**	**Spatial (m)**
Coastal Aerosol	0.443	60	Coastal Aerosol	0.43 - 0.45	30	Blue	0.45 - 0.52	30
Blue	0.49	10	Blue	0.45 - 0.51	30	Green	0.52 - 0.60	30
Green	0.56	10	Green	0.53 - 0.59	30	Red	0.63 - 0.69	30
Red	0.665	10	Red	0.64 - 0.67	30	Near Infrared	0.77 - 0.90	30
Vegetation Red Edge	0.705	20	Near Infrared (NIR)	0.85 - 0.88	30	Short-wave Infrared	1.55 - 1.75	30
Vegetation Red Edge	0.74	20	Shortwave (SWIR) 1	1.57 - 1.65	30	Thermal	10.40 - 12.50	60
Vegetation Red Edge	0.783	20	Shortwave (SWIR) 2	2.11 - 2.29	30	Mid-Infrared	2.08 - 2.35	30
Near Infra-red (NIR)	0.842	10	-	-	-	-	-	-
Vegetation Red Edge	0.865	20	-	-	-	-	-	-
SWIR	1.61	20	-	-	-	-	-	-
SWIR	2.19	20	-	-	-	-	-	-

Table 2. Band names, spectral resolution, and spatial resolution of the sensors used in the current study.

Methodology

Data preprocessing

We created multilayer rasters in the sentinel application platform (SNAP) software, using the selected bands listed in Table 2. Subsequently, 20 m and 60 m bands in Sentinel-2A/B data were resampled to a consistent 10 m spatial resolution. This allowed for consistent visualization and data processing. Although pan sharpening improves spatial resolution, we did not pan sharpen the Landsat images as it distorts spectral reflectance leading to erroneous characterization of facies (Jawak et al. 2022a). Fig. 2 illustrates the methodology of this study. Next, we normalized the data to rescale pixel values to the non-unit reflectance range between 0-1. This process allowed band-by-band comparison of the spectral reflectance for observable facies against existing literature (Luis and Singh 2020). Equation 1 presents the normalization used for both sensors which was adapted across all bands.

$$R = (\theta <= 0) \times 0 + (\theta >= n) \times 1 + (\theta > 0 \, and \, \theta < n) \times (\theta)/n \qquad \textit{Eqn. 1.}$$

where: R – Rescaled (normalized) pixel reflectivity value,
θ – is the scaled pixel value,
n – is the maximum digital number based on the radiometric resolution of the sensor.

After preprocessing, we digitized the VB glacier boundary for the year 2013 and used that boundary as a mask to extract the VB glacier area for all images. Along with providing an estimate of the change in glacier facies from 2013 to 2023, this allows for visual assessment of the thematic classification.

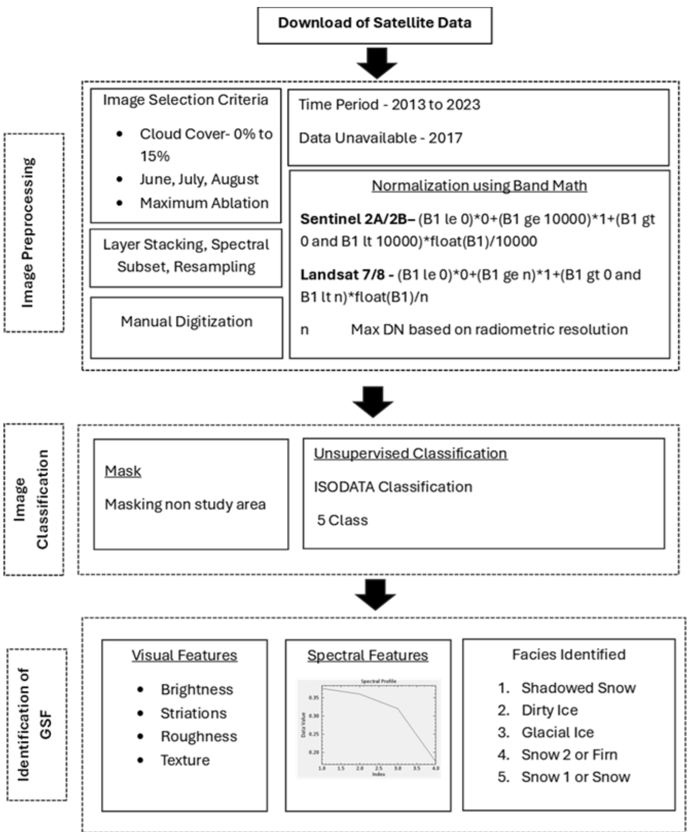

Fig. 2. The data processing methodology of the present study. *Note*: DN: Digital number; ISODATA: Iterative Self-Organizing Data Analysis Technique; GSF: Glacier surface facies.

ISODATA classification

Ouchra and Belangour (2021) suggest that image classification is crucial because it helps to visualize and extract valuable information from a satellite image. In supervised classification, the pixels of the data are characterized using training data provided by the analyst (Jawak et al. 2015). Unsupervised classification assigns thematic value without user-defined training data. These classifiers combine pixels of similar properties into thematic classes based on a predefined number of clusters. This type of classification is also known as spectral clustering. The most common types of unsupervised classification are K-means and Iterative self-organizing data analysis (ISODATA)(Jawak et al. 2015). We selected ISODATA because of its demonstrated utility for mapping GSF (Pope and Rees 2014a). Considering the terrain, existing literature, and the resolution of the data, we delimited the ISODATA classification to deliver five output classes.

Identification of glacier surface facies

Our delimitations of five classes ideally represent snow, firn, ice, shadowed snow, and dirty ice. However, based on the ISODATA clustering and evaluation of the satellite data, the classes were redesigned as:

a) *Snow or snow I* – It is the brightest facies located at the highest elevation. It presents a smooth and continuous surface without any striation. It possesses the lowest moisture and maximum reflectance among all facies (Jawak et al. 2019, 2022b).

b) *Firn or snow II* – This snow is formed by melting and refreezing (Florath et al. 2022). It is brighter than ice but lower than snow or snow 1. The lower brightness is due to the increase in moisture content. The surface is smooth and continuous like snow and is located near snow as the transition facies of snow to ice (Jawak et al. 2019, 2022b). We found that in certain imagery (excluding 2019, 2022, and 2023), firn does not visually or spectrally match established patterns reported in literature. However, it is consistently differentiated as a middle class between snow and glacier ice. Accordingly, in these cases, we labelled firn as 'snow 2' and designated the original snow class as 'snow 1'.

c) *Ice* – Ice displays flow induced striations and rough texture. Due to increased moisture content and compaction of the individual crystals, its brightness and reflectance is much lower than firn (Jawak et al. 2019, 2022b).

d) *Dirty ice* – Dirty ice is a mixed facies comprising of a mixture of dust, debris and ice (Jawak et al. 2019, 2022b). It presents a lower brightness than ice and is observed at the lowest elevations and around the glacier's margins.

e) *Shadowed snow* – Shadowed snow presents the lowest reflectance with a dark tone and a smooth surface (Jawak et al. 2019, 2022b).

Results and Discussion

To streamline the results of this experiment and maintain readability of the manuscript, we present the thematic classification maps of 2013, 2018, and 2023 (*see* Fig. 3). The maps for the rest of the temporal period (Supplementary Figs. A1-A7) are available in the Supplementary Materials.

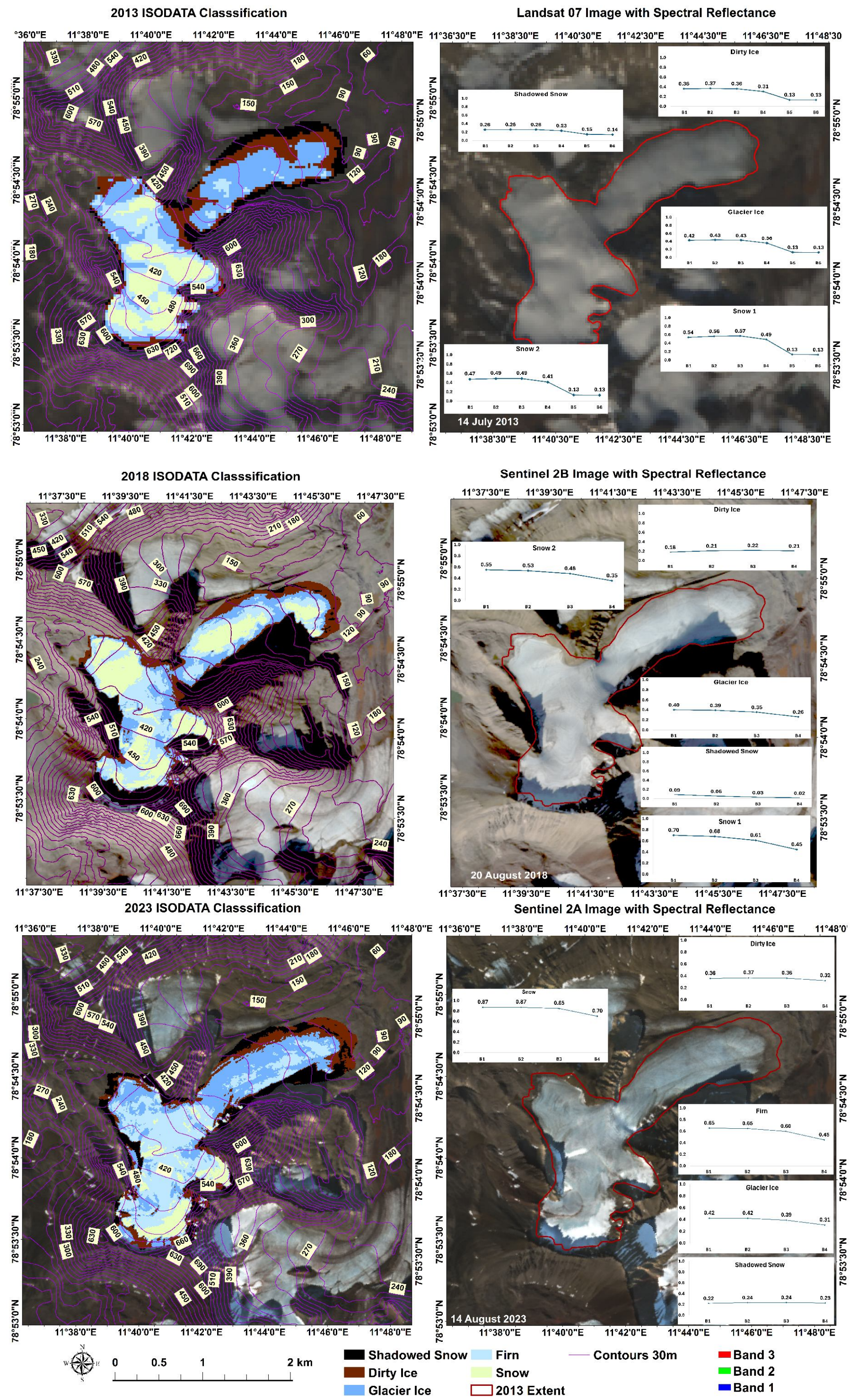

Fig. 3. Classification of the 2013 Landsat 07, 2018 Sentinel 2B, and 2023 Sentinel 2A data. The left panel presents the thematic classification, while the right displays the source data, spectral reflectance of the classified facies, date of acquisition, and the glacier extent drawn on the 2013 image. Contour lines are drawn from the ArcticDEM 2 m (Porter et al. 2022).

When assessing classification derived from unsupervised algorithms, it is necessary to determine the primary function of the assessment. In the present study, we are not aiming to create a highly accurate map, rather, we focus on understanding how untrained image properties influence spectral clustering. In the case of snow/snow 1, and firn/snow 2, coarser resolution of images from 2013 to 2018 prohibits a clear characterization of firn. Snow 2 displays lower reflectance than firn but does not present the visual and spectral characteristics typical for firn. Therefore, we categorized this as snow 2. Images from 2019-2023 permit a clearer distinction of firn (Seier et al. 2024).

Interestingly, snow/snow 1 has displayed a receding trend from 2013 to 2023, with a reduction of 0.31 km^2 from 2013 to 2023 (Fig. 4). While this behavior is typical of warming glaciated regions (Kohler et al. 2007), this trend is inverted for snow 2/firn. While delivering an area of 0.60 km^2 in 2013 for snow 2, the 2023 classification provides an area of 1.01 km^2 for the corresponding firn class. Although clearly inaccurate classification, this may be due to the overall darkening of the glacier. As observed in Fig. 3, the increase in spatial resolution provides a robust view of the darkening of the glacial surface. Thus, while snow/snow 1 is still easily characterizable by its bright appearance and high reflectivity values, snow 2/firn may provide convoluted data to the clustering algorithm. This convolution is clearly visible in the classification of shadowed snow and dirty ice.

From 2013 to 2023, glacier ice has clearly reduced, and much of the glacier terminus is converted to dirty ice. While it is possible to be categorized as debris, other areas of the glacier with low reflectance and visible dust/debris on the surface provide similar spectral reflectance as the area between the 2013 glacier boundary and the glacier ice facies. Thus, without adding an extra 'debris' class, dirty ice' should effectively encompass all areas of the glacier covered by debris, mixed with dust/debris, and this region created by the recession of glacier ice. Additionally, this increase in dirty ice should be quantifiable via an increase in its area from 2013 to 2023. However, classified dirty ice displays a reduction in area from 0.58 km^2 in 2013 to 0.49 km^2 in 2023. Moreover, shadowed snow which made up 0.44 km of the glacier in 2013, encompassed 0.49 km^2 in 2023. This suggests that although spectrally separable and visually distinct, shadowed snow and dirty ice can be misclassified (Jawak et al. 2022b) and therefore misrepresented by spectral clustering algorithms.

Glacier ice has reduced from 0.95 km^2 in 2013 to 0.85 km^2 in 2023. Shadowed snow over the glacier tongue presented a reduction in area that would be categorized into glacier ice. For reference, the 2020 Sentinel-2A image (Supplementary Fig. A5) presented low shadowed snow (0.41 km^2). In this case, ISODATA classified dirty ice at 0.55 km^2, glacial ice at 0.66 km^2, firn at 0.85 km^2, and snow at 0.63 km^2. Moreover, visual assessment of the 2020 image suggests a low misclassification between shadowed snow and dirty ice. This indicates that shadow covers are detrimental to accurate classification of facies (Jawak et al. 2019). This can be further assessed by observing the 2014 Landsat 7 (Supplementary Fig. A1) and the 2018 Sentinel-2B classifications (Fig. 3). In both these cases, shadowed snow was high, 0.82 km^2 in 2014 and 0.66 km^2 in 2018. In both cases, dirty ice displayed a low area, 0.28 km^2 in 2014 and 0.41 km^2 in 2018. Interestingly, in 2014 and 2018, glacier ice was classified at 0.50 km^2 and 0.51 km^2; snow 2 was classified at 0.80 km^2 and 0.79 km^2; and snow 1 was classified at 0.73 km^2 and 0.72 km^2. Near similar areas for all facies except dirty ice and shadowed snow suggests that increased shadow cover severely distorts classification.

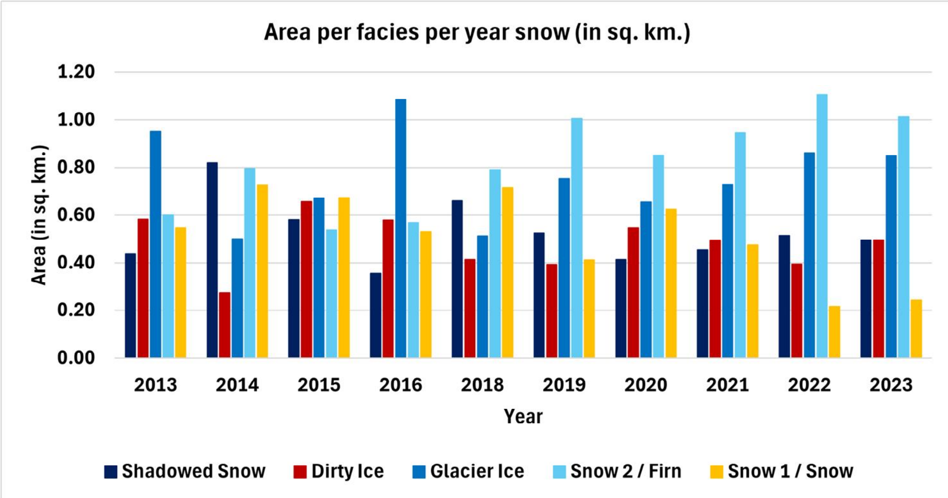

Fig. 4. Calculated area per facies from the ISODATA classification per year including shadowed snow.

Alternatively, the 2016 Landsat 8 image presented the least shadowed snow area (0.36 km^2). Here, dirty ice was classified at 0.58 km^2, glacier ice at 1.09 km^2, snow 2 at 0.57 km^2, and snow 1 at 0.53 km^2. As visible in Fig. 3, although clear differences are visible in the facies themselves, the classified area provides unreliable distortions due to shadowed snow and overall darkening of the glacier.

As information extraction techniques evolve with modern technologies, there is a significant shift towards deep learning methodologies for mapping facies (Kaushik et al. 2022). Deep learning functions primarily on reliable training data. In this study, we have demonstrated how scene to scene shifts in a simple facet of shadow cover can cause clear distortions in the spectral clustering of facies data. Even in the hands of a trained operator using object-based image analyses, textural features, and additional ancillary layers, shadow cover remains a persistent problem (Jawak et al. 2022b). GSF maps are a dynamic, sensitive, and highly effective mechanisms for monitoring glacial health as they are the direct surface manifestations of the state of snow and ice within a glacial body. However, in Svalbard, increased cloud covers due to the interaction of sea with ice (Cisek et al. 2017), daylight availability due to the polar night, and shadow cover due to illumination angles are scene to scene challenges that require effective monitoring and reporting. Careful spatiotemporal mapping of GSF in such terrain can yield valuable insight into how these distortions alter facies outputs, providing much needed information for operators and deep learning models alike. While SAR can overcome cloud and shadow errors, it is necessary to document and analyze the present challenges to effectively leverage long-term archival opportunities presented by the Landsat sensors. In future, we will conduct a carefully trained spatiotemporal mapping of GSF over a longer period to understand exact trends in facies, overall deglaciation, and identify scene to scene errors hampering long-term analyses.

Conclusion

In this study, we conducted a spatio-temporal unsupervised classification of GSF of the Vestre Brøggerbreen glacier in Ny-Ålesund, Svalbard from 2013 to 2023 using a mix of Landsat 7, Landsat 8, and Sentinel-2A/B data. We identified snow/snow 1, firn/snow 2, glacier ice, dirty ice, and shadowed snow. Although there is a clear increase in dirty ice and a reduction in glacier ice from 2013 to 2023, shadow cover prevents accurate spectral clustering of the pixels. Images with high shadow cover (2014, 2018, and 2023) display a substantial reduction in dirty ice and corresponding misrepresentation of other facies. Due to these misrepresentations, dirty ice was classified with a much lower spatial distribution in 2023 (0.49 km^2) than in 2013 (0.58 km^2). Moreover, firn/snow 2 was classified as a larger area in 2023 (1.01 km^2). The present results identify a clear challenge in spatiotemporal mapping of GSF, *i.e.* identifying, accounting, and understanding errors induced by scene/image properties. The present results are expected to inform future collection of training data for generating reliable long-term GSF archives.

References

ALI, I., SHUKLA, A. and ROMSHOO, S. A. (2017): Assessing linkages between spatial facies changes and dimensional variations of glaciers in the upper Indus Basin, western Himalaya. *Geomorphology*, 284: 115-129. doi: 10.1016/j.geomorph.2017.01.005

BENSON, C. S. (1959): Physical investigations on the snow and firn of northwest Greenland 1952, 1953, and 1954. US Army Snow Ice and Permafrost Research Establishment. *Corps of Engineers*, 26.

BRAUN, M., SCHULER, T., HOCK, R., BROWN, I. and JACKSON, M. (2007): Comparison of remote sensing derived glacier facies maps with distributed mass balance modelling at Engabreen, northern Norway. *IAHS-AISH Publication* [Preprint].

CISEK, M., MAKUCH, P. and PETELSKI, T. (2017): Comparison of meteorological conditions in Svalbard fjords: Hornsund and Kongsfjorden. *Oceanologia*, 59(4): 413-421. doi: 10.1016/j.oceano.2017.06.004

ENGESET, R. V., KOHLER, J., MELVOLD, K. and LUNDÉN, B. (2002): Change detection and monitoring of glacier mass balance and facies using ERS SAR winter images over Svalbard. *International Journal of Remote Sensing*, 23(10): 2023-2050. doi: 10.1080/01431160110075550

FLORATH, J., KELLER, S., ABARCA-DEL-RIO, R., HINZ, S., STAUB, G. and WEINMANN, M. (2022): Glacier monitoring based on multi-spectral and multi-temporal satellite data: A case study for classification with respect to different snow and ice types. *Remote Sensing*, 14(4). doi: 10.3390/rs14040845

GARCÍA-RUBIO, G., HUNTLEY, D. and RUSSELL, P. (2015): Evaluating shoreline identification using optical satellite images. *Marine Geology*, 359: 96-105. doi: 10.1016/j.margeo.2014.11.002

GARG, V., THAKUR, P. K., RAJAK, D. R., AGGARWAL, S. P. and KUMAR, P. (2022): Spatio-temporal changes in radar zones and ELA estimation of glaciers in NyÅlesund using Sentinel-1 SAR. *Polar Science*, 31: 100786. doi: 10.1016/j.polar.2021.100786

GEETHA PRIYA, M., KRISHNA, V., LOHIT, S. and DEVARAJ, S. (2022): Detecting short-term surface melt over Vestre Broggerbreen, Arctic glacier using indigenously developed unmanned air vehicles. *Geocarto International*, 37(11): 3167-3178. doi: 10.1080/10106049.2020.1849416

GREUELL, W., OERLEMANS, J. (2005): Validation of AVHRR- and MODIS-derived albedos of snow and ice surfaces by means of helicopter measurements. *Journal of Glaciology*, 51(172): 37-48. doi: 10.3189/172756505781829575

HAQ, M.A., ALSHEHRI, M., RAHAMAN, G., GHOSH, A., BARAL, P. and SHEKHAR, C. (2021): Snow and glacial feature identification using Hyperion dataset and machine learning algorithms. *Arabian Journal of Geosciences*, 14(15). doi: 10.1007/s12517-021-07434-3

ISAKSEN, K., NORDLI, Ø., FØRLAND, E.J., ŁUPIKASZA, E., EASTWOOD, S. and NIEDŹWIEDŹ, T. (2016): Recent warming on Spitsbergen – Influence of atmospheric circulation and sea ice cover. *Journal of Geophysical Research: Atmospheres*, 121(20): 11,913-11,931. doi: 10.1002/2016JD025606

JAWAK, S. D., DEVLIYAL, P. and LUIS, A. J. (2015): A comprehensive review on pixel oriented and object oriented methods for information extraction from remotely sensed satellite images with a special emphasis on cryospheric applications. *Advances in Remote Sensing*, 04(03): 177-195. doi: 10.4236/ars.2015.43015

JAWAK, S. D., WANKHEDE, S. F. and LUIS, A. J. (2019): Explorative study on mapping surface facies of selected glaciers from chandra basin, Himalaya Using WorldView-2 Data. *Remote Sensing*, 11(10). doi: 10.3390/rs11101207

JAWAK, S. D., WANKHEDE, S. F., LUIS, A. J. and BALAKRISHNA, K. (2022a): Effect of image-processing routines on geographic object-based image analysis for mapping glacier surface facies from Svalbard and the Himalayas. *Remote Sensing*, 14(17). doi: 10.3390/rs14174403

JAWAK, S. D., WANKHEDE, S. F., LUIS, A. J. and BALAKRISHNA, K. (2022b): Impact of image-processing routines on mapping glacier surface facies from Svalbard and the Himalayas using pixel-based methods. *Remote Sensing*, 14(6). doi: 10.3390/rs14061414

JAWAK, S. D., WANKHEDE, S. F., LUIS, A. J. and BALAKRISHNA, K. (2022c): Multispectral characteristics of glacier surface facies (Chandra-Bhaga Basin, Himalaya, and Ny-Ålesund, Svalbard) through investigations of pixel and object-based mapping using variable processing routines. *Remote Sensing*, 14(24). doi: 10.3390/rs14246311

JAWAK, S. D., WANKHEDE, S. F., LUIS, A. J. and BALAKRISHNA, K. (2022d): High-resolution remote sensing for mapping Glacier Facies in the Arctic. *In*: M. Pandey, P. C. Pandey, Y. Ray, A. Arora, S. D. Jawak, U. K. Shukla (eds): *Advances in Remote Sensing Technology and the Three Poles*. doi: 10.1002/9781119787754.ch26

JAWAK, S. D., WANKHEDE, S. F., PANDIT, P. H. and BALAKRISHNA, K. (2023): Spatiotemporal variations of Glacier Surface Facies (GSF) in Svalbard: An example of Midtre Lovénbreen. *Environmental Sciences Proceedings*, 29(1): 22. doi: 10.3390/ECRS2023-15840

KAR, R., MAZUMDER, A., MISHRA, K., PATIL, S. K., RAVINDRA, R., RANHOTRA, P. S., GOVIL, P., BAJPAI, R. and SINGH, K. (2018): Climatic history of Ny-Alesund region, Svalbard, over the last 19,000 yr: Insights from quartz grain microtexture and magnetic susceptibility. *Polar Science*, 18: 189-196. doi: 10.1016/j.polar.2018.04.004

KAŠTOVSKÁ, K., ELSTER, J., STIBAL, M. and ŠANTRŮČKOVÁ, H. (2005): Microbial assemblages in soil microbial succession after glacial retreat in Svalbard (High Arctic). *Microbial Ecology*, 50(3): 396-407. doi: 10.1007/s00248-005-0246-4

KAUSHIK, S., SINGH, T., BHARDWAJ, A., JOSHI, P. K. and DIETZ, A. J. (2022): Automated delineation of supraglacial debris cover using deep learning and multisource remote sensing data. *Remote Sensing*, 14(6): 1352. doi: 10.3390/rs14061352

KOHLER, J., JAMES, T. D., MURRAY, T., NUTH, C., BRANDT, O., BARRAND, N. E., AAS, H. F. and LUCKMAN, A. (2007): Acceleration in thinning rate on western Svalbard glaciers. *Geophysical Research Letters*, 34(18). doi: 10.1029/2007GL030681

LAPOINTE, F., KARMALKAR, A. V., BRADLEY, R. S., RETELLE, M. J. and WANG, F. (2024): Climate extremes in Svalbard over the last two millennia are linked to atmospheric blocking. *Nature Communications*, 15(1). doi: 10.1038/s41467-024-48603-8

LUCKMAN, A., JANSEN, D., KULESSA, B., KING, E. C., SAMMONDS, P. and BENN, D. I. (2012): Basal crevasses in Larsen C Ice Shelf and implications for their global abundance. *The Cryosphere*, 6(1): 113-123. doi: 10.5194/tc-6-113-2012

LUIS, A.J., SINGH, S. (2020): High-resolution multispectral mapping facies on glacier surface in the Arctic using WorldView-3 data. *Czech Polar Reports*, 10(1): 23-36. doi: 10.5817/CPR2020-1-3

OUCHRA, H., BELANGOUR, A. (2021): Satellite image classification methods and techniques: A survey', in *IST 2021 – IEEE International Conference on Imaging Systems and Techniques, Proceedings*. Institute of Electrical and Electronics Engineers Inc. doi: 10.1109/IST50367.2021.9651454

PATEL, L., SHARMA, P. and THAMBAN, M. (2019): Spatio-temporal variability of snow water equivalent over the Vestre Broggerbreen and Feiringbreen glaciers, Ny-Ålesund, Svalbard. *Journal of Earth System Science*, 128(7). doi: 10.1007/s12040-019-1224-4

POPE, A., WILLIS, I. C., REES, W. G., ARNOLD, N. S. and PÁLSSON, F. (2013): Combining airborne lidar and Landsat ETM+ data with photoclinometry to produce a digital elevation model for Langjökull, Iceland. *International Journal of Remote Sensing*, 34(4): 1005-1025. doi: 10.1080/01431161. 2012.705446

POPE, A., REES, G. (2014a): Using in situ spectra to explore landsat classification of glacier surfaces: *International Journal of Applied Earth Observation and Geoinformation*, 27(Part A): 42-52. doi: 10.1016/j.jag.2013.08.007

POPE, A., REES, W. G. (2014b): Impact of spatial, spectral, and radiometric properties of multispectral imagers on glacier surface classification. *Remote Sensing of Environment*, 141: 1-13. doi: 10.1016/j.rse.2013.08.028

PORTER, C., HOWAT, I., NOH, M. J., HUSBY, E., KHUVIS, S., DANISH, E., TOMKO, K., GARDINER, J., NEGRETE, A., YADAV, B., KLASSEN, J., KELLEHER, C., CLOUTIER, M., BAKKER, J., ENOS, J., ARNOLD, G., BAUER, G., and MORIN, P. (2022): "ArcticDEM – Strips, Version 4.1". Harvard Dataverse, V1, [Accessed on: 21 January 2019]. doi: 10.7910/DVN/3VDC4W

ROY, D. P., KOVALSKYY, V., ZHANG, H. K., VERMOTE, E. F., YAN, L., KUMAR, S. S. and EGOROV, A. (2016): Characterization of Landsat-7 to Landsat-8 reflective wavelength and normalized difference vegetation index continuity. *Remote Sensing of Environment*, 185: 57-70. doi: 10.1016/j.rse.2015.12.024.

SADIQ, M., DUTTA, S., KUMAR, P., JAT, S., GAJBHIYE, D. Y. and DHARWADKAR, A. (2022): Ice dynamics of Vestre Brøggerbreen glaciers, Ny-Ålesund, Svalbard, Arctic. *Journal of Earth System Science*, 131(1). doi: 10.1007/s12040-021-01750-8

SEIER, G., ABERMANN, J., WECHT, M., NEUREITER, A., SULZER, W. and KELLERER-PIRKLBAUER, A. (2024): Thinning and dynamics of the glacier terminus at the Pasterze Glacier (Austria), 2016–2021. *Cold Regions Science and Technology*, 222: 104198. doi: 10.1016/j.coldregions.2024.104198

SERREZE, M. C., BARRY, R. G. (2011): Processes and impacts of Arctic amplification: A research synthesis. *Global and Planetary Change*, 77(1–2): 85-96. doi: 10.1016/j.gloplacha.2011.03.004

SINGH, P., ROY, U. and TSUJI, M. (2016): Characterisation of yeast and filamentous fungi from Brøggerbreen glaciers, Svalbard. *Polar Record*, 52(4): 442-449. doi: 10.1017/S003224741 6000085

WANKHEDE, S. F., PANDIT, P. H., JAWAK, S. D., LUIS, A. J. and BALAKRISHNA, K. (2023): Modulating spectral reflectance and its impact on thematic mapping: An analysis on glacier facies using very high-resolution satellite imagery. *In*: SPIE-Intl Soc Optical Eng, 61 p. doi: 10.1117/12.2680310

WICKSTRÖM, S., JONASSEN, M. O., CASSANO, J. J. and VIHMA, T. (2020): Present temperature, precipitation, and rain-on-snow climate in Svalbard. *Journal of Geophysical Research: Atmospheres*, 125(14). doi: 10.1029/2019JD032155

WILLIAMS, R. S., HALL, D. K. and BENSON, C. S. (1991): Analysis of glacier facies using satellite techniques. *Journal of Glaciology*, 37(125): 120-128. doi: 10.3189/s0022143000042878

YOUSUF, B., SHUKLA, A., ALI, I., GARG, P. K. and GARG, S. (2024): Surface facies analysis of the Gangotri and neighbouring glaciers, central Himalaya. *Science of Remote Sensing*, 9: 100128. doi: 10.1016/j.srs.2024.100128

YOUSUF, B., SHUKLA, A., ARORA, M. K. and JASROTIA, A. S. (2019): Glacier facies characterization using optical satellite data: Impacts of radiometric resolution, seasonality, and surface morphology. *Progress in Physical Geography*, 43(4): 473-495. doi: 10.1177/0309133319840770

Supplementary Materials

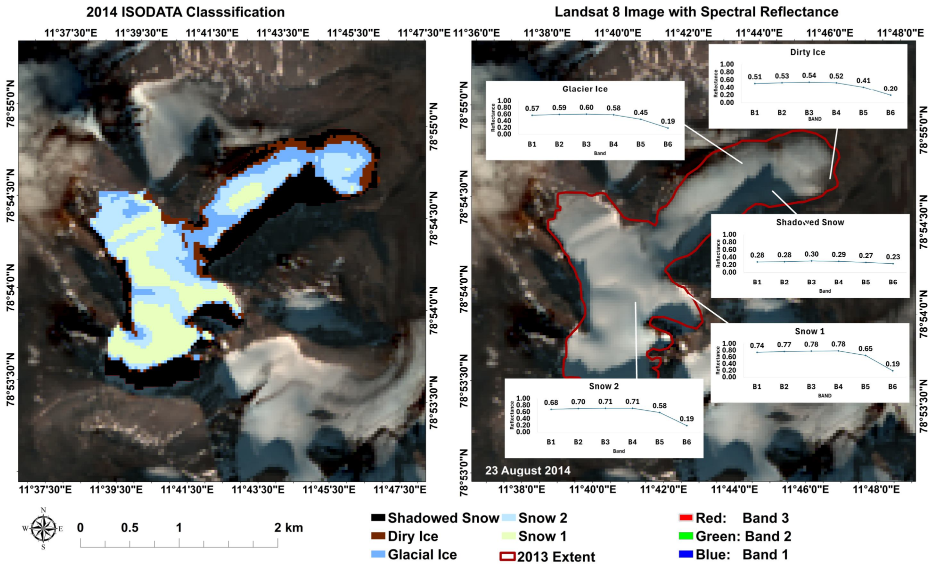

Figure A1. Classification of the 2014 Landsat 07 image. The left panel presents the thematic classification, while the right displays the source data, spectral reflectance of the classified facies, date of acquisition, and the glacier extent drawn on the 2013 image.

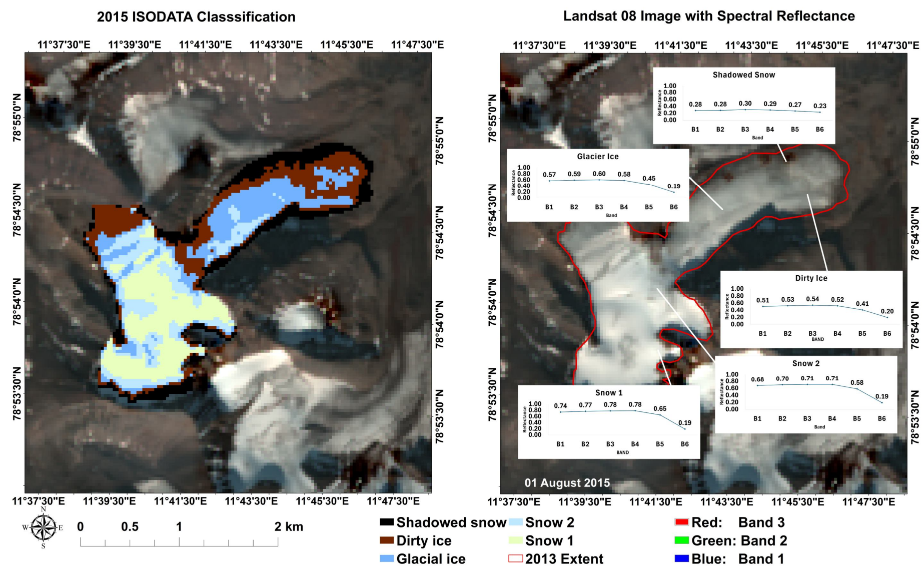

Figure A2. Classification of the 2015 Landsat 08 image. The left panel presents the thematic classification, while the right displays the source data, spectral reflectance of the classified facies, date of acquisition, and the glacier extent drawn on the 2013 image.

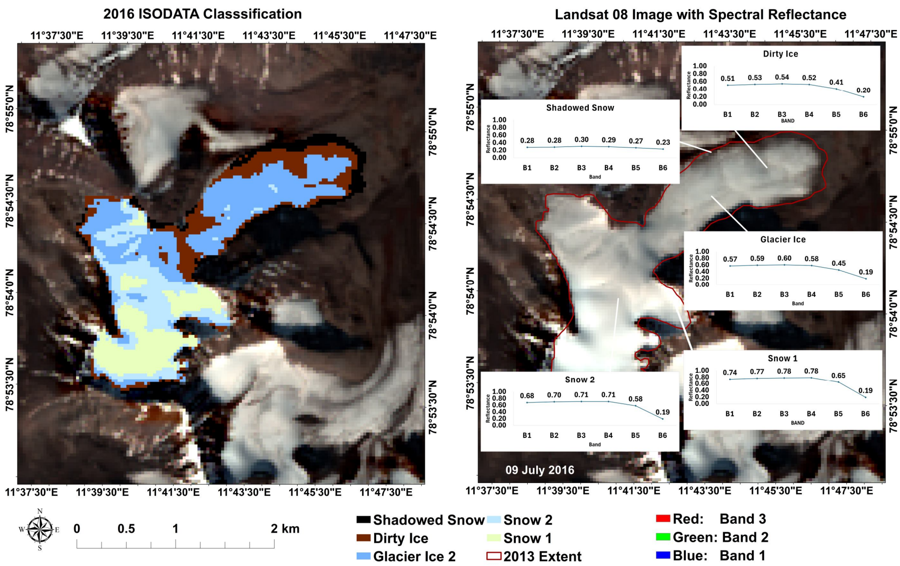

Figure A3. Classification of the 2016 Landsat 08 image. The left panel presents the thematic classification, while the right displays the source data, spectral reflectance of the classified facies, date of acquisition, and the glacier extent drawn on the 2013 image.

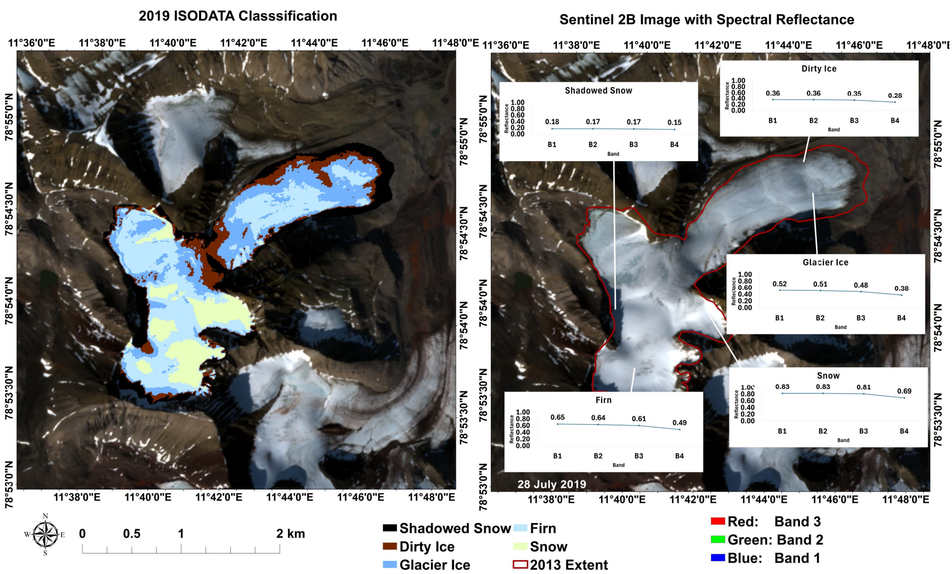

Figure A4. Classification of the 2019 Sentinel-2B image. The left panel presents the thematic classification, while the right displays the source data, spectral reflectance of the classified facies, date of acquisition, and the glacier extent drawn on the 2013 image.

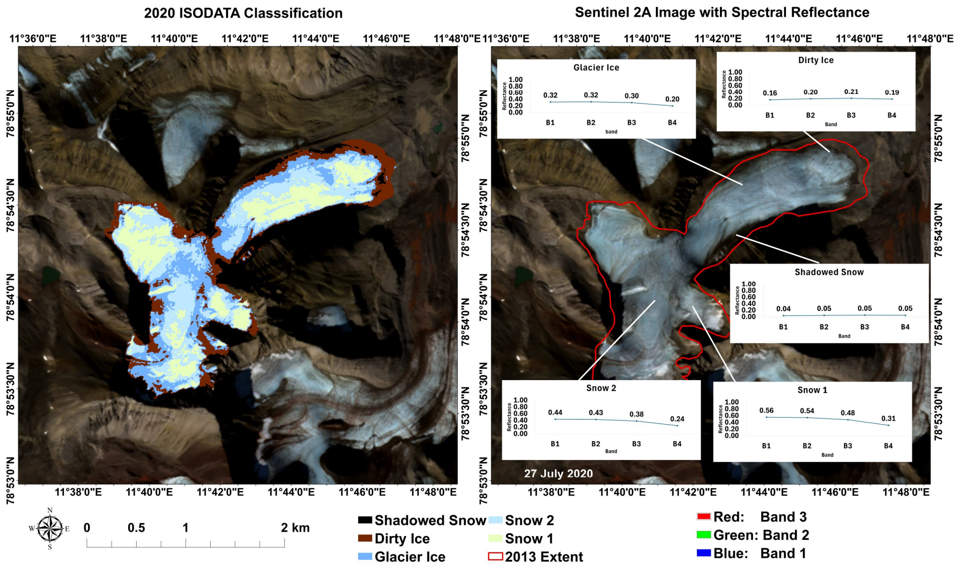

Figure A5. Classification of the 2020 Sentinel-2A image. The left panel presents the thematic classification, while the right displays the source data, spectral reflectance of the classified facies, date of acquisition, and the glacier extent drawn on the 2013 image.

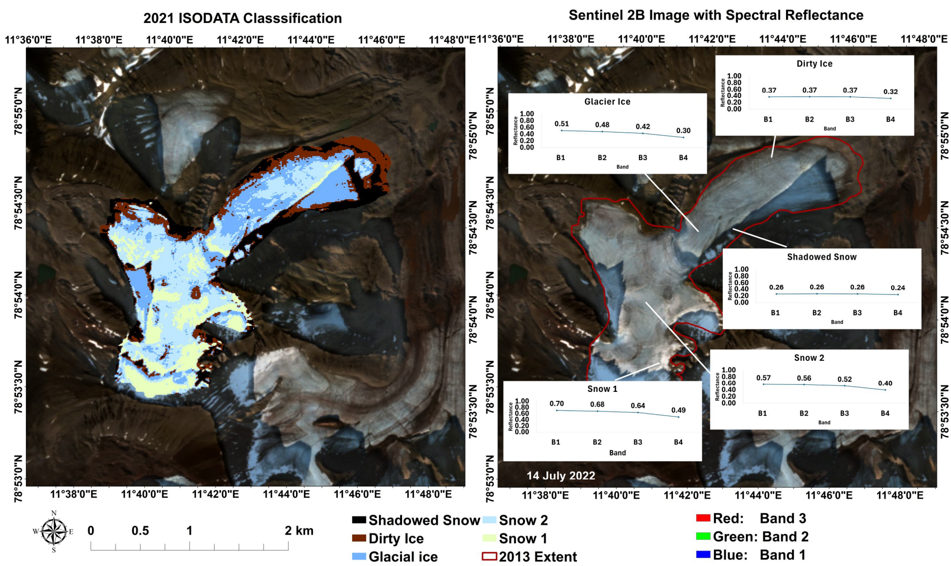

Figure A6. Classification of the 2021 Sentinel-2B image. The left panel presents the thematic classification, while the right displays the source data, spectral reflectance of the classified facies, date of acquisition, and the glacier extent drawn on the 2013 image.

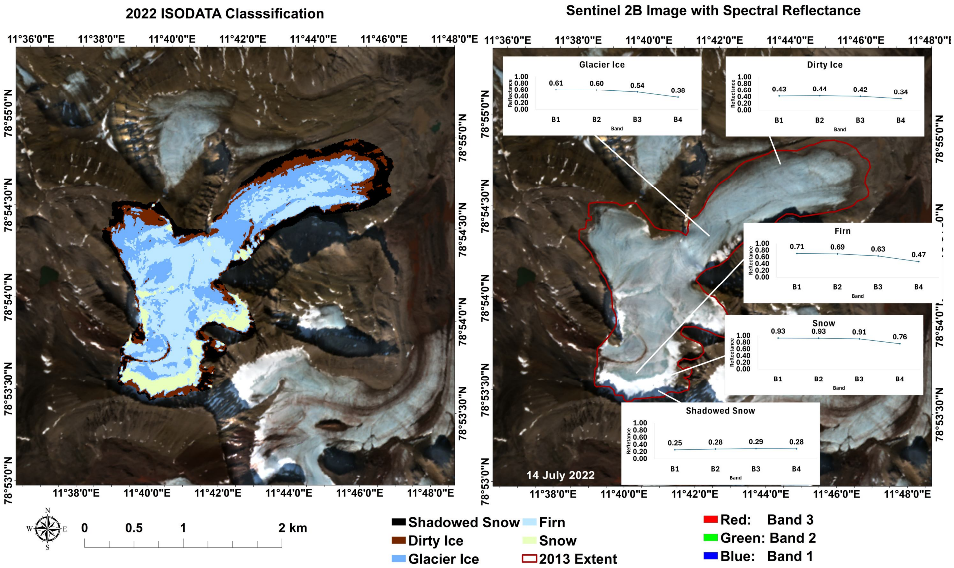

Figure A7. Classification of the 2022 Sentinel-2B image. The left panel presents the thematic classification, while the right displays the source data, spectral reflectance of the classified facies, date of acquisition, and the glacier extent drawn on the 2013 image.